Graphene-Based Photothermal Agent for Rapid and Effective Killing of Bacteria

Meng-Chin Wu,[†,§] Archana R. Deokar,[†,§] Jhan-Hong Liao,[†] Po-Yuan Shih,[‡] and Yong-Chien Ling[†,‡,*]

[†]Department of Chemistry and [‡]Institute of NanoEngineering and MicroSystems, National Tsing Hua University, Hsinchu 30013, Taiwan. [§]These authors contributed equally to this work.

ABSTRACT Conventional antibiotic therapies are becoming less efficient due to the emergence of antibiotic-resistant bacterial strains. Development of novel antibacterial material to effectively inhibit or kill bacteria is crucial. A graphene-based photothermal agent, magnetic reduced graphene oxide functionalized with glutaraldehyde (MRGOGA), was synthesized for efficient capture and effective killing of both gram-positive *Staphylococcus aureus* (*S. aureus*) and gram-negative *Escherichia coli* (*E. coli*) bacteria upon near-infrared (NIR) laser irradiation. In the present work, we took advantage of the excellent photothermal properties of reduced graphene oxide upon NIR laser irradiation and glutaraldehyde as an efficient capturing agent toward both bacteria. Its magnetic characteristic allows bacteria to be readily trapped in a small volume by the external magnet. The synergetic effects increase the heating extent by MRGOGA upon NIR laser irradiation and the killing of the captured bacteria. The survival rate and membrane integrity assay demonstrate that 80 ppm MRGOGA solution provided rapid and effective killing of up to 99% of both gram-positive and gram-negative bacteria in 10 min upon NIR laser irradiation under batch operation mode. Graphene demonstrated better photothermal antibacterial efficiency than carbon nanotubes. Furthermore, a microfluidic chip system under continuous operation mode demonstrates the reusability of MRGOGA and offers a biocompatible platform for online phothothermal sterilization.

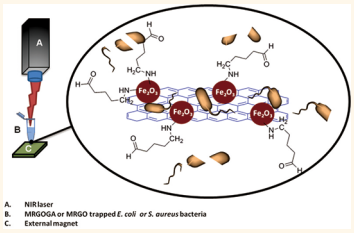

KEYWORDS: graphene · photothermal · NIR · magnetic · bacteria · sterilization

In the late 20th century, conventional antibiotic therapies were becoming less efficient owing to the emergence of antibiotic-resistant bacterial strains. The demand of developing new antibiotics and therapies for combating bacterial infections is becoming crucial. Lately, for instance, bacterial infections caused by New Delhi Metallo-β-lactamase-1 type bacteria were found to be multiple-drug-resistant, causing severe nosocomial infections worldwide, and resolving this issue should be addressed more seriously and urgently.[1] During the past decade, inorganic nanoparticles (NPs) and semiconductors have played an increasingly important role in combating bacterial infections.[2−4] Graphene, since its discovery in 2004, has drawn tremendous attention from the scientific community as a promising nanomaterial (NM) due to its multiple properties such as its unique mechanical stiffness,[5] outstanding electronic transport,[6] specific surface areas,[7] thermal stability,[8] conductivity,[9] and optical properties.[10] Various applications such as transistors,[11−13] solar cells,[14] and sensors[15] have been carried out rapidly. Recently, researchers are concentrating more on studying the biological properties of graphene because of its superior biocompatibility.[16] Biological applications of graphene include drug carriers,[17−19] biosensing,[20−22] cancer therapies,[23,24] and antimicrobial property.[25,26]

Photothermal therapy has been widely developed by combining pulsed laser and strong light-absorbing materials such as gold NPs,[27] carbon nanotubes (CNTs),[28,29] and graphene.[30] Their unique optical properties make these NMs able to absorb light irradiation and to release it as heat. NIR irradiation in the range of 700−1100 nm is the most advantageous wavelength region suitable for biological applications, due to its capability of deeper penetration into tissues.[31] The NIR laser photothermal therapy can focus on a targeted area for effective treatment. Both CNTs and graphene own similar or even identical properties, including antibacterial activities and photothermal features. Photothermal therapy

* Address correspondence to ycling@mx.nthu.edu.tw.

Received for review October 16, 2012 and accepted January 29, 2013.

Published online January 29, 2013
10.1021/nn304782d

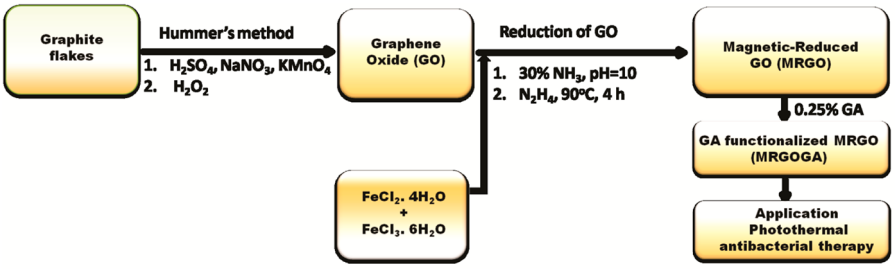

Scheme 1. Synthesis strategy of MRGOGA for photothermal antibacterial therapy.

based on CNTs has been extensively investigated for drug delivery,[32] cancer treatment,[33] and antibacterial therapy.[34,35] Recently, graphene-based NMs conjugated with NIR irradiation have been applied for anticancer treatments and drug delivery.[36,37] Markovic *et al.* demonstrated that graphene has better photothermal abilities than CNTs.[38] Graphene nanowalls deposited on stainless steel substrates were able to damage the membrane of gram-positive *S. aureus* bacteria more effectively by 1 h direct interaction with the sharp edges of nanowalls.[39] The graphene oxide/TiO_2 film demonstrated the photoinactivation of *E. coli* after 4 h irradiation under solar light.[40] Nevertheless, combining the advantage of photothermal and cross-linking capability of graphene for antibacterial utilization has not yet been explored. The NMs' capability to inactivate bacteria within a few minutes after interaction is still warranted. With this motivation, efforts were taken to synthesize a graphene-based photothermal agent, MRGOGA, for efficient capturing and effective killing of bacteria within 10 min upon NIR irradiation.

In this work, graphene oxide (GO) was reduced and integrated with superparamagnetic property by functionalizing it with magnetic NPs (MRGO, Scheme 1). We demonstrated that, by this unique magnetic feature, material−bacteria conjugates were aggregated under the external magnet quickly. Therefore, NIR irradiation could emphasize and focus on those and enhance the killing efficiency of the concentrated bacteria rather than in a dispersed state. Further, MRGO was functionalized with glutaraldehyde (GA) to yield MRGOGA, which possesses excellent cross-linking properties with proteins in bacteria and thus can be used as a capturing agent for both gram-positive and gram-negative bacteria.[41] The antibacterial efficiency of MRGOGA was carried out under batch and continuous operation modes. Under batch mode, MRGOGA was introduced to the still bacteria solution and aggregated at the bottom with the help of an external magnet and eventually subjected to NIR laser irradiation (808 nm, 1.5 W/cm^2). Under continuous mode, MRGOGA was introduced into the well of a microfluidic chip, and the bacterial solution was continuously pumped through a microfluidic chip and then eventually subjected to NIR laser irradiation at the center of the reaction well. Furthermore, a comparative photothermal antibacterial property of graphene with its structural sibling (*i.e.*, CNTs) was also studied. To our knowledge, this is the first report documenting that graphene-based photothermal agents can inactivate bacteria within a few minutes. The reusability as well as the online sterilization method of MRGOGA was also demonstrated through the utilization of a microfluidic chip system.

RESULTS AND DISCUSSION

Preparation and Characterization of MRGOGA. The synthesis of MRGOGA was carried out in three steps (Scheme 1). Graphite flakes were oxidized by Hummer's method to GO,[42] followed by simultaneous reduction and functionalization with magnetic NPs[43] to yield magnetic reduced graphene oxide MRGO and finally functionalized with GA to yield MRGOGA. By following the aforementioned procedure, single-walled CNTs (SWCNTs) were also functionalized with magnetic NPs and GA (MCNGA) for comparative photothermal antibacterial study. The morphology was examined by transmission electron microscopy (TEM). Figure 1a demonstrates the uniform distribution of the magnetic NPs on MRGO nanosheets compared with SWCNTs functionalized with magnetic NPs (Figure 1c), which might be due to the sheet-like structure of RGO. The high-resolution TEM image (HRTEM, Figure 1b,d) illustrates magnetic NPs with approximately spherical shape and size ranging from 5 to 8 nm (delineated with yellow arrows).

The Fourier transform infrared (FT-IR) spectrum of GO (Figure 2 curve a) shows O−H stretching (a broad band at 2500−3550 cm^{-1} centered around 3300 cm^{-1}), surface carboxylic groups C═O−O (1720 cm^{-1}), aromatic C═C (1620 cm^{-1}), carboxyl O═C−O (1360 cm^{-1}), epoxy C−O (1225 cm^{-1}), and alkoxy C−O (1050 cm^{-1}). The FT-IR spectrum of MRGO (Figure 2 curve b) reveals that aromatic alkene C═C (1570 cm^{-1}) and C−O (1200 cm^{-1}) are the only remaining functional groups, demonstrating that most oxygen functionalities have successfully been reduced. The Fe−O bond (575 cm^{-1}) and amine N−H broad band (3000−3550 cm^{-1} centered at 3391 cm^{-1}) confirm the magnetic functionalities of RGO. The FT-IR spectrum of MRGOGA (Figure 2 curve c) reveals the appearance of C−N stretching (1200−1030 cm^{-1}) presumably due to the imine (R_2C═NR) bond formed between aldehyde (−C(═O)H) groups of

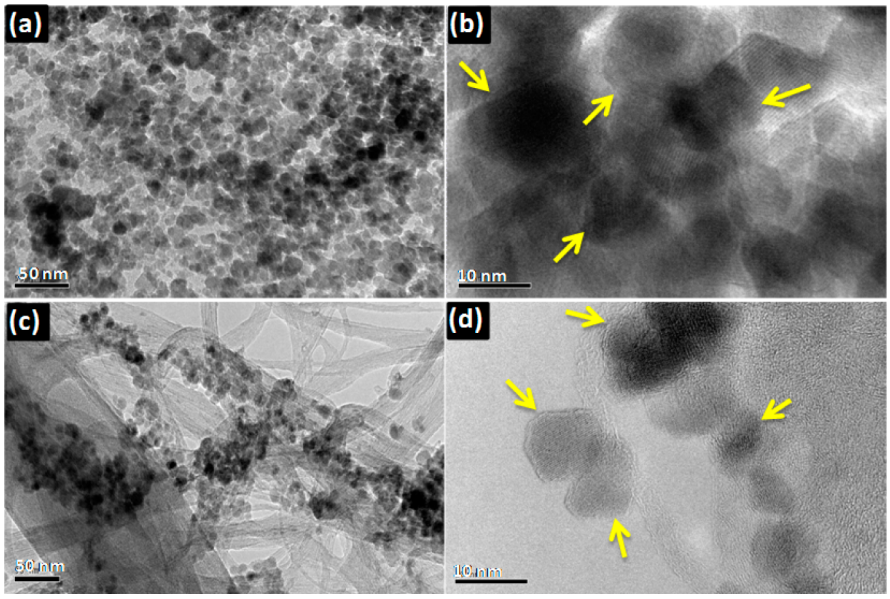

Figure 1. TEM images of (a) MRGO and (c) MCN, and HRTEM images of magnetic NPs on (b) RGO nanosheets and (d) SWCNTs.

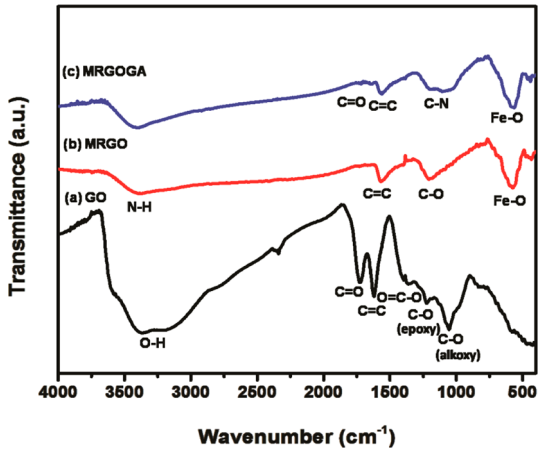

Figure 2. FT-IR spectra of (a) GO, (b) MRGO, and (c) MRGOGA.

glutaraldehyde and amine ($-NH_2$) groups of MRGO. The FT-IR spectra verified the change of functional groups during the transition from GO to MRGOGA.

The magnetic properties of MRGOGA were investigated using a superconducting quantum interference device (SQUID). Figure 3a demonstrates MRGOGA exhibiting good superparamagnetic property with a saturation magnetization value (M_s) ~26 emu g^{-1} at 298 K, very low coercivity (H_c) ~8 O_e, and remnant magnetization (M_r) ~0.56 emu g^{-1}. Figure 3b presents the photograph of two vials filled with solution with a magnet attached to the outside of both vials. The solution in the left vial contains well-dispersed GO and retains its brown color. In contrast, the solution in the right vial contains MRGOGA and becomes colorless. The MRGOGA aggregated (within 1 min) onto the vial wall by an external magnetic field.

The optical absorption of MRGO, MRGOGA, and MCNGA was investigated using a UV–vis–NIR solid-state spectrometer. MRGO, MRGOGA, and MCNGA (Figure 4a) exhibit optical absorption from the UV to the NIR region with 0.03, 0.44, and 0.18 absorbance at 808 nm, respectively. The GA not only captured bacteria but also cooperated to increase the optical absorption of MRGO to MRGOGA in the NIR region (Figure 4a). The temperature evolution profile (Figure 4b) represents the photothermal efficiency of MRGO, MRGOGA, and MCNGA upon NIR laser (808 nm 1.5W/cm^2, 10 min) irradiation as a function of time. The PBS buffer was utilized as a control and had virtually no change (Figure 4b) in temperature (from 26 to 28 °C), whereas the MRGOGA solution showed drastic change in temperature from ~26 to 50 °C in 10 min, which was relatively higher than that of MRGO from ~26 to 43 °C and MCNGA from ~26 to 42 °C. On average, the temperature change of the MRGOGA solution was around 1.4 and 1.5 times faster than that of MRGO and MCNGA, respectively. Notably, it rises exponentially every 2 min (Supporting Information, Table S1). Three different concentrations (20, 40, and 80 ppm) were studied to investigate the light to heat conversion efficiency of MRGOGA (Supporting Information, Figure S3), and 80 ppm MRGOGA demonstrated better photothermal efficiency (~26 to 50 °C) compared to 20/40 ppm MRGOGA (Supporting Information, Figures S3 and S4).

Bacteria Capturing Capabilities. The antibacterial activities of MRGO, MRGOGA, and MCNGA were tested against both bacterial strains and evaluated on the basis of respective contribution from cross-linking and photothermal ability. The MRGO nanosheets were functionalized with GA, which acted as a cross-linking agent toward bacterial cell walls. The GA possesses excellent cross-linking capability with peptidoglycan on bacterial cell walls and proteins.[44]

The optical density at 600 nm (OD_{600}) indicates the density of bacteria in a medium.[45] We therefore used

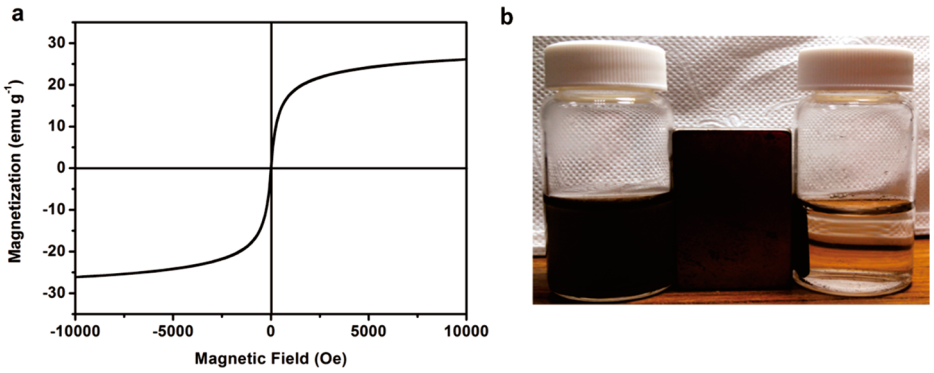

Figure 3. (a) Hysteresis curve of MRGOGA at 300 K. (b) Photograph of vials filled with solution containing GO (left) and aggregated MRGOGA (right). A magnet was attached to the outside of the two vials.

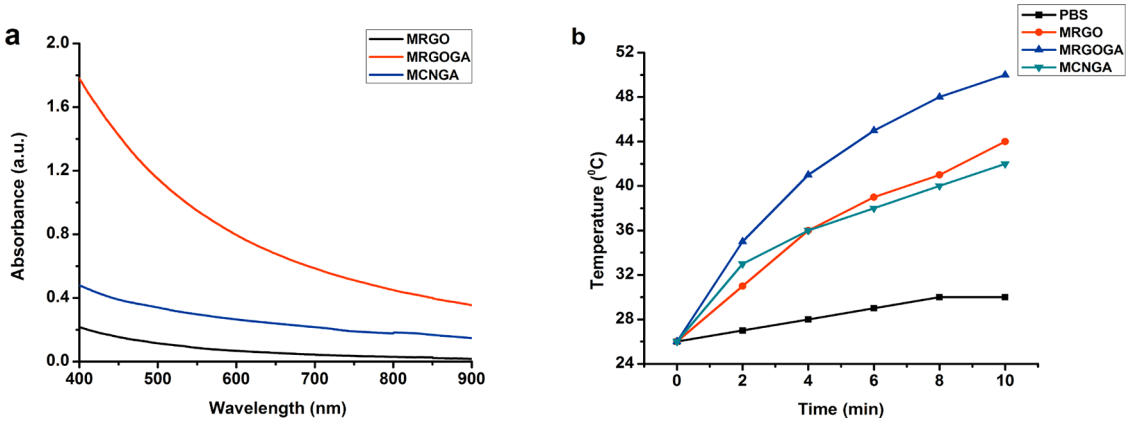

Figure 4. (a) UV−vis−NIR spectra of 80 ppm MRGO, MCNGA, and MRGOGA solution. (b) Temperature evolution profile of PBS, and 80 ppm MRGO, MCNGA, and MRGOGA solution upon NIR laser (808 nm, 1.5 W/cm^2) irradiation.

OD_{600} of the suspension to represent bacteria capturing capabilities. The absorption evolution profiles (Figure 5) reveal that the OD_{600} did not decrease during the mixing process with MRGO for both bacterial strains, implying that MRGO did not possess any bacteria capturing capability. The bacteria concentration in suspension still remained high. In contrast, the absorption dramatically dropped after mixing with MRGOGA and MCNGA (Figure 5). In the case of MRGOGA, OD_{600} for *S. aureus* decreased from 1.203 to 0.125 (Figure 5a) and for *E. coli* from 1.541 to 0.396 (Figure 5b), whereas in the case of MCNGA, OD_{600} for *S. aureus* decreased from 1.180 to 0.397 (Figure 5a) and for *E. coli* from 1.600 to 0.683 (Figure 5b). The solution became clear shortly after MRGOGA/MCNGA was trapped by an external magnet. The results demonstrated excellent capturing capability by MRGOGA toward both bacterial strains compared with MCNGA. Notably, the capturing capability is not affected by the outer membrane in gram-negative bacteria. The results are in accordance with scanning electron microscopy (SEM) (Figure 6). Both bacterial strains (Figure 6, delineated with yellow arrows) were efficiently captured by MRGOGA (Figure 6, delineated with red arrows) owing to its unique magnetic and sheet-like structural properties combined with the cross-linking ability of GA.

Antibacterial Photothermal Treatment. The efficiency of antibacterial photothermal treatment by MRGOGA under two operation modes was investigated using the schematic illustrated in Figure 7. The batch mode was operated with a still bacteria solution (Figure 7a), whereas the continuous mode was operated with a flowing bacteria solution being continuously pumped through a microfluidic chip system (Figure 7b).

Table 1 lists the survival rate (%) in triplicate measurements of both bacterial strains (original concentration 10^6−10^7 CFU/mL) after 10 min interaction with 80 ppm MRGO, MRGOGA, and MCNGA solution under dark and NIR laser irradiation conditions, respectively. Under dark, the survival rates were all above 100%, suggesting that both bacteria strains were not affected by MRGO, MRGOGA, and MCNGA, implying that when MRGO (and MRGOGA/MCNGA) was applied alone, a 10 min interaction time was insufficient to produce significant bacterial damage. The bacteria were still growing during this period.

Under NIR laser irradiation, the bacteria survival rate in the absence of photothermal agents was still above 100%, indicating that NIR laser irradiation alone was harmless to both bacterial strains (Supporting Information, Figures S6 and S7). In contrast, the bacteria survival

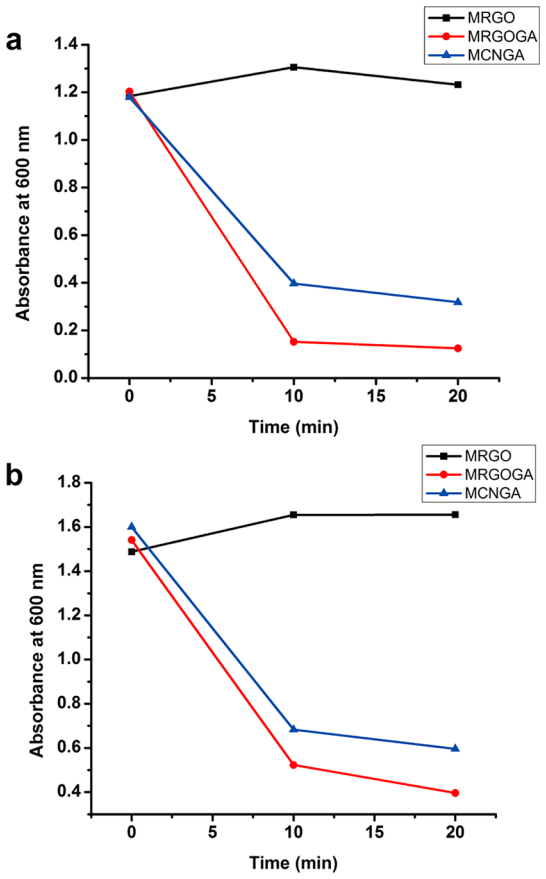

Figure 5. Bacteria capturing capabilities of MRGO, MRGOGA, and MCNGA represented by OD_{600} for (a) gram-positive *S. aureus* and (b) gram-negative *E. coli*.

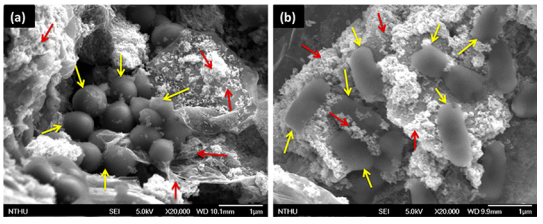

Figure 6. SEM images of MRGOGA (red arrows) capturing (a) gram-positive *S. aureus* (yellow arrows) and (b) gram-negative *E. coli* bacteria (yellow arrows).

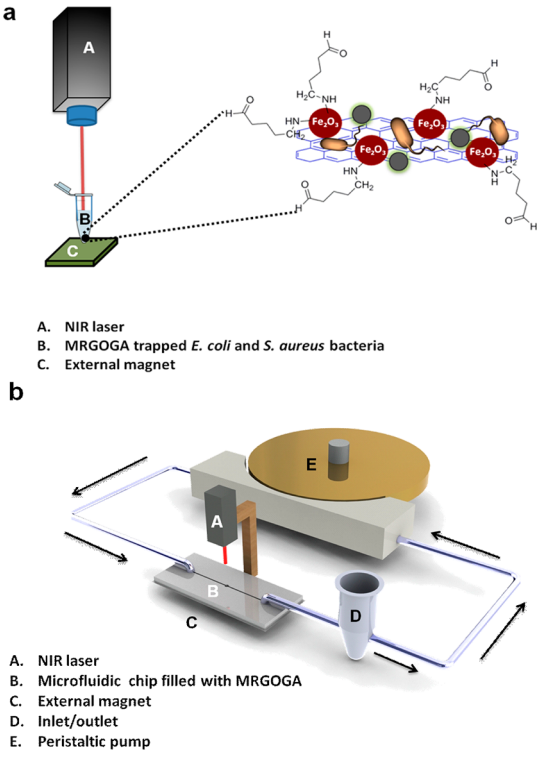

Figure 7. Schematic of (a) batch and (b) continuous operation mode for antibacterial photothermal treatment by MRGOGA.

TABLE 1. Survival rate of *S. aureus* and *E. coli* for 80 ppm MRGO, MRGOGA, and MCNGA Solution after Photothermal Treatments under Batch Operation Mode

	survival rate (%) $n = 3$			
	under dark		NIR laser irradiation	
agent	*S. aureus*	*E. coli*	*S. aureus*	*E. coli*
none			155 ± 15	102 ± 14
MRGO	143 ± 50	117 ± 34	45 ± 14	39 ± 12
MRGOGA	147 ± 20	108 ± 15	0.4 ± 0.1	0.1 ± 0.1
MCNGA	110 ± 9	133 ± 32	8.7 ± 2	20 ± 6

rate in 80 ppm MRGO (and MRGOGA/MCNGA) solution dramatically decreased upon NIR laser irradiation onto the aggregated conjugate formed by applying an external magnet. There is a significant difference in antibacterial efficiencies between MRGO and MRGOGA. Fewer bacteria were killed after photothermal treatment with MRGO (Table 1 and Supporting Information, Figure S6) as it was not able to capture both bacterial strains. Most bacteria were still suspended in solution and could not be trapped to one spot by the external magnet, hence weakening the photothermal efficiency of the NIR laser irradiation. Nevertheless, 80 ppm MRGO solution still showed photothermal property but much less than MRGOGA as demonstrated by the corresponding solid-state UV–vis–NIR spectra (Figure 4) and bacteria capturing capabilities (Figure 5). The lack of bacteria capturing functional groups and lower photothermal efficiency of MRGO might be responsible for its ineffective killing of both strains. Several investigations have demonstrated excellent antibacterial activities by graphene. The minimum time for interacting with bacteria is at least 1 h (Supporting Information, Table S2).[39,46] Our approach yielded similarly excellent antibacterial efficiency with an interacting time as low as 10 min. Moreover, MRGOGA demonstrated better antibacterial efficiency toward both bacteria as compared to MCNGA owing to its high bacteria capturing capability and light to heat conversion ability. MCNGA shows better antibacterial activity toward gram-positive *S. aureus* bacteria than

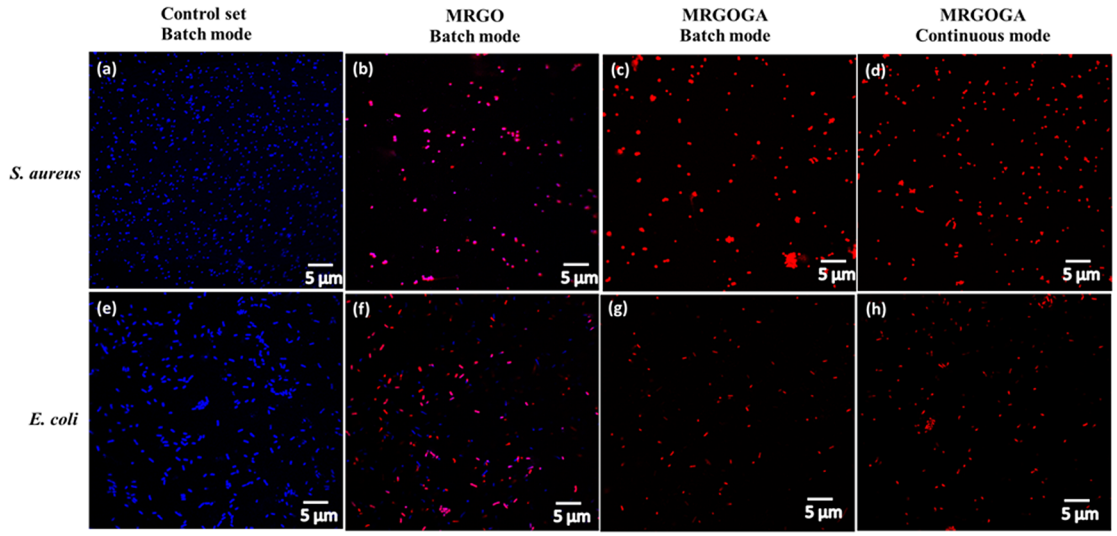

Figure 8. CLSM images of *S. aureus* (top row) and *E. coli* (bottom row) by various photothermal treatments. (a,e) In the absence photothermal agents; (b,f) with 80 ppm MRGO solution operated under batch mode; (c,g) with 80 ppm MRGOGA solution operated under batch mode; (d,h) with MRGOGA operated under continuous mode.

gram-negative *E. coli*. This might be due to resistance of the outer membrane in gram-negative bacteria.

We further carried out a fluorescence-based cell viability assay to verify the bacteria survival rate. Membrane-impermeant propidium iodide (PI) labels dead bacteria with red fluorescence, whereas membrane-permeant 4′-6-diamidino 2-phenylindole (DAPI) labels live bacteria with blue fluorescence. Similar fluorescence dye methods have been applied in SWCNT-based toxicity studies.[47] The confocal laser scanning microscopy (CLSM) images of *S. aureus* (Figure 8a) and *E. coli* (Figure 8e) clearly evidenced abundant amount of DAPI-labeled live bacteria in the absence of photothermal agents. Both DAPI-labeled (live bacteria) and membrane-impermeant PI-labeled (dead bacteria) bacterial strains became apparent in the MRGO solution (Figure 8b,f) after 10 min of NIR laser irradiation operated under batch mode, and this is consistent with the survival rate (Table 1). On the other hand, under similar operational conditions, only PI-labeled dead bacteria became apparent for both bacterial strains in the MRGOGA solution (Figure 8c,g), demonstrating better killing efficiency by MRGOGA toward both bacterial strains. CLSM images of the continuous operation mode (Figure 8d,h) appear to be contrary to the survival rate (Supporting Information, Table S4), whereas CLSM images under batch operation mode (Figure 8c,g) are consistent with bacteria survival rates listed in Table 1.

The excellent bacteria capturing capability by MRGOGA synergistically increased its photothermal effectiveness, and a rate of up to 99% bacteria killing efficiency was obtained after 10 min of NIR laser irradiation. The MRGOGA is a superior photothermal agent for killing both gram-positive and gram-negative bacteria, compared to previously reported graphene-based antibacterial materials (Supporting Information, Table S2).[48,49] The key factors toward effective killing of bacteria include the capturing ability of GA and photothermal effects by graphene, which is capable of absorbing irradiated light and subsequently releasing the energy as heat.[50,51] A moderate temperature such as ~37 °C is required for mesophile bacteria growth. Heat produced by MRGOGA upon NIR laser irradiation raised the solution temperature to ~50 °C. At this temperature, the enzymes were denatured and would inhibit necessary intracellular reactions, damage proteins and lipids on the cell membrane, and finally lead to bacterial death. Moreover, the MRGOGA cross-linked bacteria can be easily controlled by an external magnetic field and aggregated at small volumes, allowing efficient use of NIR laser irradiation to increase local heating for effective bacteria killing.

Furthermore, we observed that the survival rate of *E. coli* is lower than *S. aureus* (Table 1 and Supporting Information, Figures S6 and S7), implying the photothermal treatment is more effective toward *E. coli*. The increased efficiency could be attributed to the difference in heat sensitivity between *E. coli* and *S. aureus*. Gram-positive bacteria exhibit better heat resistance than gram-negative ones.[52] The *D* value (*i.e.*, decimal reduction time in microbiology) was used to compare the relative heat resistance between microorganisms and showed *S. aureus* exhibiting better heat resistance than *E. coli*.[53] Therefore, although the bacteria capturing capacities are relatively similar for both bacterial strains, the lower heat resistance of *E. coli* might explain its lower survival rate.

We used a home-designed microfluidic chip system (Figure 7b) to investigate the reusability of MRGOGA for antibacterial photothermal treatment operated under continuous mode. The system provides a biocompatible platform for investigating chemical and

biological processes with a relatively small amount of fluid. The chip is made of polydimethylsiloxane (PDMS), the most commonly used polymer for manufacturing microfluidic chips. PDMS is used for its unique properties of being chemically inert, nontoxic, stretchable, and flexible for design. Moreover, it exhibits high transmittance of light which makes it a perfect material for photothermal treatment.[54] The continuous mode was operated by connecting the microfluidic chip to a peristaltic pump (Figure 7). The system parameters are described in the Methods section. The reaction well in the chip was filled with MRGOGA first, and five different batches of bacteria were subsequently pumped through the system continuously. The survival rate in % for *S. aureus* (Supporting Information, Table S4) [3 (minimum survival rate) − 6 (maximum survival rate), 5 (average) ± 1 (SD)] and *E. coli* [10 (minimum survival rate) − 13 (maximum survival rate), 12 (average) ± 1 (SD)] remained low even after five rounds of continuous photothermal treatments by MRGOGA (Supporting Information, Table S4 and Figure S8). The killing efficiencies of the continuous mode were lower than that of the batch mode (Table 1, Figure 8, and Supporting Information, Figures S7 and S8) and better with regard to *S. aureus*. The result is exactly opposite to that of the batch mode, presumably due to the difference in the interacting process between bacteria and MRGOGA under different operating modes. Under the batch operation mode, the bacteria were continuously mixed with homogenously dispersed MRGOGA in the solution *via* vortex for 10 min. The MRGOGA was able to efficiently capture bacteria and therefore exhibited better killing efficiency. Under the continuous operation mode, the bacteria capturing capability could be lowered by noncomplete contact between MRGOGA and bacteria. In addition, *E. coli* are rod-shaped and bigger than *S. aureus*, which made them harder to capture by a solid form of MRGOGA in the continuous system.

In vivo applications of graphene-based NMs are still in the infancy stage. Surface functionalization plays a critical role in the biocompatibility. In the case of MRGOGA, RGO was functionalized with magnetic NPs and GA, hence it can reduce the strong hydrophobic interactions of graphene with cells/tissues. It has been shown that the surface functionlization can lead to a reduction of reactive oxygen species, which mediate apoptosis though caspase-3 activation.[55] On the other hand, another important consideration for *in vivo* application of graphene-based nanomaterial which still remains is the clearance after their intravenous injection since graphene is nondegradable and long-term toxicity may be a concern.[56] Normal Chinese hamster ovary cells (CHO-K1) are the commonly used cell line not only for cytotoxicity studies but also for genotoxicity.[57] The cytotoxicity of MRGO and MRGOGA was investigated using MTT assay on CHO-K1 by examining the cell viabilities at various concentrations (10, 20, 50, and 100 μg/mL) for 48 h (Supporting Information, Figure S9). For *in vivo* biomedical applications of MRGOGA, it was important to study its prolonged effect; therefore, 48 h of implication time was chosen. After 48 h incubation in 100 μg/mL MRGO or MRGOGA solutions, both agents show good biocompatibilities. CHO-K1's cell viabilities were all above 100% at each MRGO concentration and slightly decreased to 87% with increased MRGOGA concentration at 100 μg/mL, presumably due to the presence of more functional groups (aldehyde groups in glutaraldehyde) on MRGOGA than MRGO. Nevertheless, the MTT assay results demonstrate the low cytotoxicity and biocompatibility of both MRGO and MRGOGA.

CONCLUSIONS

We have demonstrated MRGOGA as a rapid (within 10 min) and effective (99% killing efficiency) photothermal agent toward both gram-positive *S. aureus* and gram-negative *E. coli* bacteria compared with MCNGA under NIR laser irradiation. The MRGOGA not only possesses a good superparamagnetic property (M_s = ~26 emu g^{-1}) and optical absorption from UV to NIR regions but also exhibits efficient capturing capacity owing to the cross-linking ability of glutaraldehyde and effective killing efficiency of the photothermal ability of graphene toward both bacterial strains. The rapid and effective antibacterial activity as well as the UV to NIR region absorption property might make a MRGOGA-based antibacterial coating work under normal solar light. The utilization of a microfluidic chip system combined with the reusability property of MRGOGA provides a biocompatible platform for online photothermal sterilization. Furthermore, the magnetic and low cytotoxity properties of MRGOGA make it an ideal candidate for *in vivo* biomedical applications because of the advantages of easy mobilization at targeted position and minimum cellular damage.

METHODS

Synthesis of GO. GO was synthesized according to Hummer's method through the oxidation of graphite flakes (Purity 99%, Alfa Aesar, USA).[38] A conical flask equipped with a magnetic stirring bar was charged with H_2SO_4 (69 mL) and cooled at 0−5 °C. Graphite flakes (1.5 g) were then added slowly with vigorous stirring, followed by adding slowly $KMnO_4$ (4.5 g) and $NaNO_3$ (1.5 g) over 15 min. The temperature of the reaction mixture was maintained at 0−5 °C during the addition process. The mixture was allowed to warm to room temperature (RT) and stirred for 1 h. The RT mixture was charged with distilled water (DI) (120 mL) and stirred for 30 min while the temperature was increased to 90 °C. The mixture was poured into DI water (300 mL), followed by slow addition of 10 mL of H_2O_2. The solution color subsequently changed from dark-brown to yellow. The remaining solution was filtered. The residual material was redispersed in water,

washed with DI water, and stopped when the filtrate pH became neutral. The resultant GO material was dried in a vacuum desiccator overnight at RT.

Synthesis of MRGOGA. GO (0.35 g) was exfoliated in DI water by sonication. Iron(III) chloride hexahydrate ($FeCl_3 \cdot 6H_2O$, 0.35 g) and iron(II) chloride tetrahydrate ($FeCl_2 \cdot 4H_2O$, 0.2 g) (purity 99%, Merck, Germany) at a ratio of 2:1 used as Fe source were dissolved in DI water (50 mL) and added slowly into the GO suspension. The ammonia solution (0.5 mL) was added quickly to the solution and stirred for 1 h at 60 °C to yield magnetic NP precipitate. Five hundred microliters of hydrazine was added to reduce GO to RGO for 4 h at 90 °C. The MRGO product was washed with DI water three times and dried in a freeze-dryer overnight. The GA was functionalized onto MRGO by dispersing MRGO (250 mg) in DI water by sonication. GA (0.25%) was then added to the solution and stirred at RT for 24 h. The MRGOGA product was collected and washed with DI water three times and dried in a freeze-dryer overnight.

Synthesis of MCNGA. The pristine SWCNTs (Timesnano, China) synthesized by the chemical vapor deposition method were acid-functionalized by a microwave-assisted method using a microwave oven (MARS-Xpress, CEM, USA) to improve the SWCNTs' dispersibility in water. An aliquot of SWCNTs (50 mg) was allowed to react with concentrated HNO_3 (5 mL, 15.8 M) in a closed Teflon bottle operated at 600 W and 180 °C for 30 min. Further, acid-functionalized SWCNTs were intergrated with magnetic NPs and GA by following a similar procedure for the aforementioned synthesis of MRGOGA.

Characterization of MRGOGA. Physical and chemical properties of MRGOGA were characterized by PXRD, FT-IR, UV−vis−NIR, Raman, SQUID, and TEM. PXRD patterns were recorded on a Rigaku D/MAX-2500 diffractometer with Cu Kα radiation (λ = 0.1540 nm). FT-IR was recorded on a Perkin-Elmer system 2000 FT-IR. UV−vis−NIR spectra were carried out using a JASCO V-570 spectrometer. Raman spectra were recorded on a Horiba spectrometer with 514 nm wavelength incident laser light. Magnetic properties were measured using a MPMS5 Quantum Design SQUID at 300 K over a range of applied fields from −10 000 to 10 000 Oe. The morphology and size were investigated using a JEOL JEM-2100 TEM at an accelerating voltage of 200 kV. The SEM images of captured bacteria were measured with a JEOL, JSM-7000F SEM.

Fabrication of the Microfluidic Chip. The pattern in the microfluidic chip was designed using Solid Works software. The template for the pattern was carved on a polymethylmethacrylate (PMMA) substrate by a three-axis computer numerical control mechanical engraver. The polydimethylsiloxane (PDMS) was filled into the PMMA template to form a solidified PDMS chip at 90 °C for 30 min. Oxygen plasma was finally used as glue to assemble the whole microfluidic chip. Parameters of the microfluidic chip such as width of channel, diameter of the reaction well, and flow rate were fixed at 500 μm, 4.5 mm, and 300 μL/min, respectively.

Bacteria Culture. Before each microbiological experiment, all samples and glassware were sterilized by autoclaving at 120 °C for 10 min. Cultures of gram-positive BCRC 11863 *S. aureus* and gram-negative BCRC 11509 *E. coli* (FIRDI, Taiwan) bacterial strains were grown on nutrient agar overnight, transferred into an Erlenmeyer flask containing nutrient broth (Scharlau Chemie, Spain) at an initial optical density (OD_{600}) of 0.1 at 600 nm, and allowed to grow at 37 °C under 200 rpm rotation. When the cultures reached an OD_{600} of 0.3 (the beginning of the logarithmic phase), they were centrifuged and washed twice with 0.9% saline solution to yield a final bacterial concentration of approximately $\sim 10^6-10^7$ CFU/mL. Turbidity measurements were carried out to monitor the bacteria capturing capabilities of MRGOGA and MCNGA. OD_{600} was used to estimate bacteria concentration of in the medium. Typically, 50 mg of MRGOGA and MCNGA was added to 5 mL of bacterial suspension. After every 10 min of vortex, MRGOGA and MCNGA along with the captured bacteria were aggregated at the bottom by an external magnet. The bacteria in suspension were finally subjected to turbidity measurement.

Assessment of Photothermal Treatment. Antibacterial efficiency was investigated under two operation modes. The batch mode was operated with a still bacteria solution, whereas the continuous mode was operated by continuously pumping the bacteria through the microfluidic chip system. Under batch mode, both *S. aureus* and *E. coli* bacteria were suspended in a PBS buffer and diluted to a final concentration of $\sim 10^6$ CFU/mL. Subsequently, 200 μL of bacteria ($\sim 10^6$ CFU/mL) was mixed with 1 mL of 80 ppm MRGO, MRGOGA, and MCNGA solution. The interaction between MRGO/MRGOGA/MCNGA and bacteria was carried out by vortexing for 10 min. The MRGO/MRGOGA/MCNGA bacteria conjugates were aggregated at the bottom with the help of an external magnet. The conjugate was immediately subjected to NIR laser irradiation (808 nm, 1.5 W/cm^2) for 10 min at a distance of 7 cm. Exact optical power of laser used in our experiment was calibrated and measured by a Newport optical power meter (USA). Finally, 100 μL of conjugate solution was collected, diluted 50 times, spread on agar plates, and incubated for 24 h at 37 °C. The control set was prepared by diluting 200 μL of bacteria to 1 mL with DI water and spread on agar plates. Under continuous mode, the microfluidic chip system coupled to a peristaltic pump was employed to maintain the bacteria solution flowing in a circular fashion. An external magnet was placed just beneath the well filled with 1 mg of MRGOGA to ensure it would not flow away with the bacterial stream. An aliquot of 800 μL of bacteria solution ($\sim 10^6$ CFU bacteria) was driven by the peristaltic pump which generated a stream flowing into the microfluidic chip. The NIR laser was focused onto the center of reaction well at a distance of 7 cm for a few seconds while 800 μL of bacteria solution continuously circulated in the system. For the material reusability test, the experiment was repeated five times consecutively with a fresh batch of bacteria in the chip system but without replacing the filled MRGOGA. The entire chip system was cleaned with DI water between each round of experiment. Eventually, 100 μL of bacteria solution was collected, diluted 50 times, spread on agar plates, and incubated for 24 h at 37 °C. The control set allowed 800 μL of bacteria solution flowing through the blank chip without MRGOGA.

Electron Microscopy Measurement. Bacterial strains exposed to 80 ppm MRGOGA solution were fixed with 4% formaldehyde in PBS, stained with 1% osmium tertraoxide (Electron Microscopic Sciences, USA), dehydrated, and subjected to SEM measurement.

Integrity of Cell Membranes Based on Fluorescence Assay. After 10 min photothermal treatment with MRGOGA solution, both *S. aureus* and *E. coli* bacteria were stained with PI (10 μg/mL) for 10 min and counterstained with DAPI (3 μg/mL) for 5 min in the dark for CSLM measurement. The live and dead bacterial cells were visualized (under a 100× lens) with a CLSM confocal microscope (Zeiss, LSM 700) equipped with an InGaN semiconductor laser (405 nm), an Ar laser (488 nm), and a He−Ne laser (543 nm).

MTT Assay. Two hundred microliters of CHO-K1 cell-containing solution ($\sim 2 \times 10^4$ cells/mL) was added to each well of a 24-well plate and incubated 1 day to allow it to adhere on the surface of the plate. Aliquots of a PBS buffer solution containing different concentrations of MRGO and MRGOGA were added to the 24-well plate, and the cell solutions were incubated for another 48 h. A 50 μL aliquot of an MTT aqueous solution (0.5 mg/mL) was added to each well of the 24-well plate 4 h before termination of the 3 day incubation, and the cells were allowed to incubate for another 4 h. Then, the upper layer of the solutions in the 24-well plate was discarded, and 1 mL of DMSO was added to each well to lyse the cell membrane followed by pipet stirring. The final solution in each well was centrifuged at 13 000 rpm to remove any solid residues before measurements of the optical absorbance at 570 nm. The optical absorbances were converted to cell viabilities based on a standard curve (absorbance *vs* cell numbers) obtained from control experiments carried out under the same condition except that no MRGO and MRGOGA were added during cell culture processes.

Conflict of Interest: The authors declare no competing financial interest.

Acknowledgment. We gratefully acknowledge the National Science Council of Taiwan (NSC 101-2627-M-007-005 and NSC-101-2113-M-007-006-MY3) and National Tsing Hua University (99N2454E1) for generous funding support. We also gratefully acknowledge Prof. L.Y. Lin from Department of Life Science, National Tsing Hua University, for fruitful discussion on MTT assay.

Supporting Information Available: XRD patterns, Raman spectra of MRGOGA, temperature evolution profile of 20, 40, and 80 ppm MRGOGA, temperature evolution profile of 40 and 80 ppm of MRGOGA and MCNGA, temperature evolution profile of 80 ppm GO and MRGOGA, MTT assay on normal Chinese hamster ovary cells (CHO-K1) in the presence of various (10, 20, 50, and 100 μg/mL) concentrations of MRGO or MRGOGA, photographs of *S. aureus* and *E. coli* after photothermal treatments with MRGO or MRGOGA under batch and continuous mode for 10 min, table of temperature change (ΔT) upon 10 min NIR laser irradiation, comparison for graphene-based antibacterial material with current study, survival rate of *S. aureus* and *E. coli* for 40 ppm MRGOGA and MCNGA, and survival rate of *S. aureus* and *E. coli* after employing photothermal therapy integrated with a dynamic microfluidic system for five consecutive rounds under continuous operation mode. This material is available free of charge *via* the Internet at http://pubs.acs.org.

REFERENCES AND NOTES

1. Kumarasamy, K. K.; Toleman, M. A.; Walsh, T. R.; Bagaria, J.; Butt, F.; Balakrishnan, R.; Chaudhary, U.; Doumith, M.; Giske, C. G.; Irfan, S.; *et al.* Emergence of a New Antibiotic Resistance Mechanism in India, Pakistan, and the UK: A Molecular, Biological, and Epidemiological Study. *Lancet Infect. Dis.* **2010**, *10*, 597–602.
2. Tian, J.; Wong, K. K. Y.; Ho, C. M.; Lok, C. N.; Yu, W. Y.; Che, C. M.; Chiu, J. F.; Tam, P. K. H. Topical Delivery of Silver Nanoparticles Promotes Wound Healing. *ChemMedChem* **2007**, *2*, 129–136.
3. Huang, W. C.; Tsai, P. J.; Chen, Y. C. Multifunctional Fe_3O_4@Au Nanoeggs as Photothermal Agents for Selective Killing of Nosocomial and Antibiotic-Resistant Bacteria. *Small* **2009**, *5*, 51–56.
4. Applerot, G.; Lipovsky, A.; Dror, R.; Perkas, N.; Nitzan, Y.; Lubart, R.; Gedanken, A. Enhanced Antibacterial Activity of Nanocrystalline ZnO Due to Increased ROS-Mediated Cell Injury. *Adv. Funct. Mater.* **2009**, *19*, 842–852.
5. Dikin, D. A.; Stankovich, S.; Zimney, E. J.; Piner, R. D.; Dommett, G. H. B.; Evmenenko, G.; Nguyen, S. T.; Ruoff, R. S. Preparation and Characterization of Graphene Oxide Paper. *Nature* **2007**, *448*, 457–460.
6. Novoselov, K. S.; Geim, A. K.; Morozov, S. V.; Jiang, D.; Zhang, Y.; Dubonos, S. V.; Grigorieva, I. V.; Firsov, A. A. Electric Field Effect in Atomically Thin Carbon Films. *Science* **2004**, *306*, 666–669.
7. Korkut, S.; Roy-Mayhew, J. D.; Dabbs, D. M.; Milius, D. L.; Aksay, I. A. High Surface Area Tapes Produced with Functionalized Graphene. *ACS Nano* **2011**, *5*, 5214–5222.
8. Wu, Z. S.; Ren, W. C.; Gao, L. B.; Zhao, J. P.; Chen, Z. P.; Liu, B. L.; Tang, D. M.; Yu, B.; Jiang, C. B.; Cheng, H. M. Synthesis of Graphene Sheets with High Electrical Conductivity and Good Thermal Stability by Hydrogen Arc Discharge Exfoliation. *ACS Nano* **2009**, *3*, 411–417.
9. Balandin, A. A.; Ghosh, S.; Bao, W. Z.; Calizo, I.; Teweldebrhan, D.; Miao, F.; Lau, C. N. Superior Thermal Conductivity of Single-Layer Graphene. *Nano Lett.* **2008**, *8*, 902–907.
10. An, X. H.; Butler, T. W.; Washington, M.; Nayak, S. K.; Kar, S. Optical and Sensing Properties of 1-Pyrenecarboxylic Acid-Functionalized Graphene Films Laminated on Polydimethylsiloxane Membranes. *ACS Nano* **2011**, *5*, 1003–1011.
11. Eda, G.; Fanchini, G.; Chhowalla, M. Large-Area Ultrathin Films of Reduced Graphene Oxide as a Transparent and Flexible Electronic Material. *Nat. Nanotechnol.* **2008**, *3*, 270–274.
12. Wang, X. M.; Xie, W. G.; Du, J.; Wang, C. L.; Zhao, N.; Xu, J. B. Graphene/Metal Contacts: Bistable States and Novel Memory Devices. *Adv. Mater.* **2012**, *24*, 2614–2619.
13. Lin, Y. M.; Jenkins, K. A.; Valdes-Garcia, A.; Small, J. P.; Farmer, D. B.; Avouris, P. Operation of Graphene Transistors at Gigahertz Frequencies. *Nano Lett.* **2009**, *9*, 422–426.
14. Tang, Y. B.; Lee, C. S.; Xu, J.; Liu, Z. T.; Chen, Z. H.; He, Z. B.; Cao, Y. L.; Yuan, G. D.; Song, H. S.; Chen, L. M.; *et al.* Incorporation of Graphenes in Nanostructured TiO_2 Films *via* Molecular Grafting for Dye-Sensitized Solar Cell Application. *ACS Nano* **2010**, *4*, 3482–3488.
15. Ang, P. K.; Chen, W.; Wee, A. T. S.; Loh, K. P. Solution-Gated Epitaxial Graphene as pH Sensor. *J. Am. Chem. Soc.* **2008**, *130*, 14392–14393.
16. Chen, H.; Muller, M. B.; Gilmore, K. J.; Wallace, G. G.; Li, D. Mechanically Strong, Electrically Conductive, and Biocompatible Graphene Paper. *Adv. Mater.* **2008**, *20*, 3557–3561.
17. Liu, Z.; Robinson, J. T.; Sun, X. M.; Dai, H. J. PEGylated Nanographene Oxide for Delivery of Water-Insoluble Cancer Drugs. *J. Am. Chem. Soc.* **2008**, *130*, 10876–10877.
18. Sun, X. M.; Liu, Z.; Welsher, K.; Robinson, J. T.; Goodwin, A.; Zaric, S.; Dai, H. J. Nano-Graphene Oxide for Cellular Imaging and Drug Delivery. *Nano. Res.* **2008**, *1*, 203–212.
19. Zhang, L. M.; Xia, J. G.; Zhao, Q. H.; Liu, L. W.; Zhang, Z. J. Functional Graphene Oxide as a Nanocarrier for Controlled Loading and Targeted Delivery of Mixed Anticancer Drugs. *Small* **2010**, *6*, 537–544.
20. Jung, J. H.; Cheon, D. S.; Liu, F.; Lee, K. B.; Seo, T. S. A Graphene Oxide Based Immuno-Biosensor for Pathogen Detection. *Angew. Chem., Int. Ed.* **2010**, *49*, 5708–5711.
21. Zhou, M.; Zhai, Y. M.; Dong, S. J. Electrochemical Sensing and Biosensing Platform Based on Chemically Reduced Graphene Oxide. *Anal. Chem.* **2009**, *81*, 5603–5613.
22. Huang, Y. X.; Dong, X. C.; Liu, Y. X.; Li, L. J.; Chen, P. Graphene-Based Biosensors for Detection of Bacteria and Their Metabolic Activities. *J. Mater. Chem.* **2011**, *21*, 12358–12362.
23. Yang, K.; Zhang, S.; Zhang, G.; Sun, X.; Lee, S.-T.; Liu, Z. Graphene In Mice: Ultrahigh *In Vivo* Tumor Uptake and Efficient Photothermal Therapy. *Nano Lett.* **2010**, *10*, 3318–3323.
24. Ma, X. X.; Tao, H. Q.; Yang, K.; Feng, L. Z.; Cheng, L.; Shi, X. Z.; Li, Y. G.; Guo, L.; Liu, Z. A. Functionalized Graphene Oxide-Iron Oxide Nanocomposite for Magnetically Targeted Drug Delivery, Photothermal Therapy, and Magnetic Resonance Imaging. *Nano Res.* **2012**, *5*, 199–212.
25. Akhavan, O.; Ghaderi, E.; Esfandiar, A. Wrapping Bacteria by Graphene Nanosheets for Isolation from Environment, Reactivation by Sonication, and Inactivation by Near-Infrared Irradiation. *J. Phys. Chem. B* **2011**, *115*, 6279–6288.
26. Liu, S. B.; Zeng, T. H.; Hofmann, M.; Burcombe, E.; Wei, J.; Jiang, R. R.; Kong, J.; Chen, Y. Antibacterial Activity of Graphite, Graphite Oxide, Graphene Oxide, and Reduced Graphene Oxide: Membrane and Oxidative Stress. *ACS Nano* **2011**, *5*, 6971–6980.
27. Huang, X. H.; Jain, P. K.; El-Sayed, I. H.; El-Sayed, M. A. Gold Nanoparticles: Interesting Optical Properties and Recent Applications In Cancer Diagnostic and Therapy. *Nanomedicine* **2007**, *2*, 681–693.
28. Kam, N. W. S.; O'Connell, M.; Wisdom, J. A.; Dai, H. J. Carbon Nanotubes as Multifunctional Biological Transporters and Near-Infrared Agents for Selective Cancer Cell Destruction. *Proc. Natl. Acad. Sci. U.S.A.* **2005**, *102*, 11600–11605.
29. Kim, J. W.; Shashkov, E. V.; Galanzha, E. I.; Kotagiri, N.; Zharov, V. P. Photothermal Antimicrobial Nanotherapy and Nanodiagnostics with Self-Assembling Carbon Nanotube Clusters. *Lasers. Surg. Med.* **2007**, *39*, 622–634.
30. Sherlock, S. P.; Tabakman, S. M.; Xie, L. M.; Dai, H. J. Photothermally Enhanced Drug Delivery by Ultrasmall Multifunctional FeCo/Graphitic Shell Nanocrystals. *ACS Nano* **2011**, *5*, 1505–1512.
31. Weissleder, R. A Clearer Vision for *In Vivo* Imaging. *Nat. Biotechnol.* **2001**, *19*, 316–317.
32. Moon, H. K.; Lee, S. H.; Choi, H. C. *In Vivo* Near-Infrared Mediated Tumor Destruction by Photothermal Effect of Carbon Nanotubes. *ACS Nano* **2009**, *3*, 3707–3713.
33. Kang, B.; Yu, D. C.; Dai, Y. D.; Chang, S. Q.; Chen, D.; Ding, Y. T. Cancer-Cell Targeting and Photoacoustic Therapy Using Carbon Nanotubes as "Bomb" Agents. *Small* **2009**, *5*, 1292–1301.
34. Liu, X.; Yu, L. M.; Liu, F.; Sheng, L. M.; An, K.; Chen, H. X.; Zhao, X. L. Preparation of Ag-Fe-Decorated Single-Walled Carbon Nanotubes by Arc Discharge and Their Antibacterial Effect. *J. Mater. Sci.* **2012**, *47*, 6086–6094.

35. Kang, S.; Pinault, M.; Pfefferle, L. D.; Elimelech, M. Single-Walled Carbon Nanotubes Exhibit Strong Antimicrobial Activity. *Langmuir* **2007**, *23*, 8670–8673.
36. Tian, B.; Wang, C.; Zhang, S.; Feng, L. Z.; Liu, Z. Photothermally Enhanced Photodynamic Therapy Delivered by Nano-Graphene Oxide. *ACS Nano* **2011**, *5*, 7000–7009.
37. Zhang, W.; Guo, Z. Y.; Huang, D. Q.; Liu, Z. M.; Guo, X.; Zhong, H. Q. Synergistic Effect of Chemo-Photothermal Therapy Using PEGylated Graphene Oxide. *Biomaterials* **2011**, *32*, 8555–8561.
38. Markovic, Z. M.; Harhaji-Trajkovic, L. M.; Todorovic-Markovic, B. M.; Kepic, D. P.; Arsikin, K. M.; Jovanovic, S. P.; Pantovic, A. C.; Dramicanin, M. D.; Trajkovic, V. S. *In Vitro* Comparison of the Photothermal Anticancer Activity of Graphene Nanoparticles and Carbon Nanotubes. *Biomaterials* **2011**, *32*, 1121–1129.
39. Akhavan, O.; Ghaderi, E. Toxicity of Graphene and Graphene Oxide Nanowalls against Bacteria. *ACS Nano* **2010**, *4*, 5731–5736.
40. Akhavan, O.; Ghaderi, E. Photocatalytic Reduction of Graphene Oxide Nanosheets on TiO_2 Thin Film for Photoinactivation of Bacteria in Solar Light Irradiation. *J. Phys. Chem. C* **2009**, *113*, 20214–20220.
41. Gorman, S. P.; Scott, E. M.; Russell, A. D. Anti-Microbial Activity, Uses and Mechanism of Action of Glutaraldehyde. *J. Appl. Bacteriol.* **1980**, *48*, 161–190.
42. Wang, S.; Tang, L. A. L.; Bao, Q. L.; Lin, M.; Deng, S. Z.; Goh, B. M.; Loh, K. P. Room-Temperature Synthesis of Soluble Carbon Nanotubes by the Sonication of Graphene Oxide Nanosheets. *J. Am. Chem. Soc.* **2009**, *131*, 16832–16837.
43. Chandra, V.; Park, J.; Chun, Y.; Lee, J. W.; Hwang, I. C.; Kim, K. S. Water-Dispersible Magnetite-Reduced Graphene Oxide Composites for Arsenic Removal. *ACS Nano* **2010**, *4*, 3979–3986.
44. Borick, P. M.; Dondersh, F. H.; Chandler, V. L. Alkalinized Glutaraldehyde New Antimicrobial Agent. *J. Pharm. Sci.* **1964**, *53*, 1273–1275.
45. Nester, E. W; Anderson, D. G; Jr. Roberts, C. E.; Nester, M. T. Microscopy and Cell Structure. In *Microbiology: A Human Perspective*; Peterson, K. A., Ed.; McGraw-Hill: New York, 2007; pp 55−82.
46. Hu, W. B.; Peng, C.; Luo, W. J.; Lv, M.; Li, X. M.; Li, D.; Huang, Q.; Fan, C. H. Graphene-Based Antibacterial Paper. *ACS Nano* **2010**, *4*, 4317–4323.
47. Liu, S. B.; Wei, L.; Hao, L.; Fang, N.; Chang, M. W.; Xu, R.; Yang, Y. H.; Chen, Y. Sharper and Faster "Nano Darts" Kill More Bacteria: A Study of Antibacterial Activity of Individually Dispersed Pristine Single-Walled Carbon Nanotube. *ACS Nano* **2009**, *3*, 3891–3902.
48. Ma, J. Z.; Zhang, J. T.; Xiong, Z. G.; Yong, Y.; Zhao, X. S. Preparation, Characterization and Antibacterial Properties of Silver-Modified Graphene Oxide. *J. Mater. Chem.* **2011**, *21*, 3350–3352.
49. Shen, J. F.; Shi, M.; Li, N.; Yan, B.; Ma, H. W.; Hu, Y. Z.; Ye, M. X. Facile Synthesis and Application of Ag-Chemically Converted Graphene Nanocomposite. *Nano. Res.* **2010**, *3*, 339–349.
50. You, J.; Shao, R.; Wei, X.; Gupta, S.; Li, C. Near-Infrared Light Triggers Release of Paclitaxel from Biodegradable Microspheres: Photothermal Effect and Enhanced Antitumor Activity. *Small* **2010**, *6*, 1022–1031.
51. Choi, K. H.; Lee, H. J.; Park, B. J.; Wang, K. K.; Shin, E. P.; Park, J. C.; Kim, Y. K.; Oh, M. K.; Kim, Y. R. Photosensitizer and Vancomycin-Conjugated Novel Multifunctional Magnetic Particles as Photoinactivation Agents for Selective Killing of Pathogenic Bacteria. *Chem. Commun.* **2012**, *48*, 4591–4593.
52. Adams, M. R.; Moss, M. O. *Food Microbiology*; RSC Publishing: Cambridge, UK, 2008.
53. Kennedy, J.; Blair, I. S.; McDowell, D. A.; Bolton, D. J. An Investigation of the Thermal Inactivation of *Staphylococcus aureus* and the Potential for Increased Thermotolerance as a Result of Chilled Storage. *J. Appl. Microbiol.* **2005**, *99*, 1229–1235.
54. Belanger, M. C.; Marois, Y. Hemocompatibility, Biocompatibility, Inflammatory and *In Vivo* Studies of Primary Reference Materials Low-Density Polyethylene and Polydimethylsiloxane: A Review. *J. Biomed. Mater. Res.* **2001**, *58*, 467–477.
55. Sasidharan, A.; Panchakarla, L. S.; Chandran, P.; Menon, D.; Nair, S.; Rao, C. N. R.; Koyakutty, M. Differential Nano-Bio Interactions and Toxicity Effects of Pristine *vs* Functionalized Graphene. *Nanoscale* **2011**, *3*, 2461–2464.
56. Zhang, Y.; Nayak, T. R.; Hong, H.; Cai, W. B. Graphene: A Versatile Nanoplatform for Biomedical Applications. *Nanoscale* **2012**, *4*, 3833–3842.
57. Di Virgilio, A. L.; Reigosa, M.; Arnal, P. M.; de Mele, M. F. L. Comparative Study of the Cytotoxic and Genotoxic Effects of Titanium Oxide and Aluminium Oxide Nanoparticles in Chinese Hamster Ovary (CHO-K1) Cells. *J. Hazard. Mater.* **2010**, *177*, 711–718.